



A Theory of a Spot

Niayesh Afshordi

*Perimeter Institute for Theoretical Physics, Waterloo, Ontario N2L 2Y5, Canada, and
Department of Physics and Astronomy, University of Waterloo, 200 University Avenue
West, Waterloo, ON, N2L 3G1, Canada*

E-mail: nafshordi@perimeterinstitute.ca

Anže Slosar

Brookhaven National Laboratory, Upton, NY 11973, USA

E-mail: anze@bnl.gov

Yi Wang

Physics Department, McGill University, Montreal, H3A 2T8, Canada

E-mail: wangyi@hep.physics.mcgill.ca

ABSTRACT: We present a simple inflationary scenario that can produce arbitrarily large spherical underdense or overdense regions embedded in a standard Λ cold dark matter paradigm, which we refer to as bubbles. We analyze the effect such bubbles would have on the Cosmic Microwave Background (CMB). For super-horizon sized bubble in the vicinity of the last scattering surface, a signal is imprinted onto CMB via a combination of Sachs-Wolfe and an early integrated Sachs-Wolfe (ISW) effects. Smaller, sub-horizon sized bubbles at lower redshifts (during matter domination and later) can imprint secondary anisotropies on the CMB via Rees-Sciama, late-time ISW and Ostriker-Vishniac effects. Our scenario, and arguably most similar inflationary models, produce bubbles which are over/underdense in potential: in density such bubbles are characterized by having a distinct wall with the interior staying at the cosmic mean density. We show that such models can potentially, with only moderate fine tuning, explain the *cold spot*, a non-Gaussian feature identified in the Wilkinson Microwave Anisotropy Probe (WMAP) data by several authors. However, more detailed comparisons with current and future CMB data are necessary to confirm (or rule out) this scenario.

KEYWORDS: cold spot, multi-stream inflation, cosmic microwave background, secondary anisotropies.

Contents

| | |
|---|-----------|
| 1. Introduction | 1 |
| 2. Cold spot and proposed explanations | 2 |
| 3. Bubble blowing in multi-stream inflation | 2 |
| 4. Effects of cosmic bubbles on the CMB | 5 |
| 4.1 Superhorizon bubbles: Sachs-Wolfe and early ISW effects | 6 |
| 4.2 Subhorizon bubbles: Late-time ISW and Rees-Sciama effects | 8 |
| 4.3 Subhorizon bubbles: Ostriker-Vishniac effect | 10 |
| 5. Comparison with Cold Spot | 12 |
| 6. Conclusions and Future Prospects | 14 |

1. Introduction

Standard inflationary theory predicts that the primordial curvature fluctuations are normally distributed [1, 2, 3, 4, 5]. At the level of linear perturbation theory this dictates that other observables, such as temperature fluctuations in the cosmic microwave background (CMB) should also be normally distributed. This has been confirmed to hold in the real data with exquisite precision [6, 7].

However, a number of interesting features are present in the data that seems to indicate a departure from the minimal inflationary scenario. Wilkinson Map Anisotropy Probe (WMAP) [8] received a special attention from scientific treasure hunters, since it is the only available full sky map of the CMB. In addition to the cold spot [9] (discussed in more detail below), various authors have found low multipole alignments [10, 11, 12, 13], north-south asymmetries [14, 15] and various other non-Gaussian features found by blind searches [16, 17]. However, the statistical significance of the results is difficult to ascertain, due to publication bias and a-posteriori nature of some of the claims presented in the literature [18, 19].

This paper is inspired by the so called *cold spot*, a nearly-circular region of the CMB that is allegedly too cold to be generated by standard Gaussian inflationary perturbations. We discuss a generic family of inflationary models/scenarios, as a generalized version of multi-stream inflation [20, 21], which can produce large spherical regions that have an offset in the potential with respect to the surrounding universe. We enumerate possible effects that such models would have on the cosmic microwave background.

These models are thus capable of reproducing the cold spot observed in the CMB data, if the bubble is either in the line of sight to the surface of last scattering or actually embedded in the surface of the last scattering. We structure the paper as follows: In Section 2 we discuss the detection of the cold spot and the proposed explanations in the literature. In the subsequent section 3 we develop our theory and show that it can fit observations without excessive fine tuning (Section 4 and Section 5). Section 6 concludes this article.

2. Cold spot and proposed explanations

The cold spot was identified and named in [9], after [22] found a detection of non-Gaussianity in the first year WMAP data [23] using Spherical Mexican Hat Wavelets [24]. The detection significance was about three sigma (about 0.1% probability). The analysis was performed on 15 arbitrary wavelet scales and two estimators, skewness and kurtosis, were used. This indicates a dilution factor due to a-posteriori detection by a factor of 30 (assuming tests are uncorrelated), lowering the detection threshold to a bit over two sigma. Later analysis confirmed this, and estimated that the a-priori detection significance is about 1.9%. [25]. The cold spot was also identified using other techniques: using more sophisticated wavelet techniques [26], steerable wavelets [27], needlets [28] and scalar indices [29]. On the other hand [30] argue that the spot is not statistically significant. Searches were performed looking for underdensity of astrophysical objects at the location of the spot using radio sources and galaxies and found no significant detection[31, 32, 33].

The cold spot was found to be almost circular with angular radius of about 4° , temperature decrement of $70 \mu K$, and independent of the frequency [34].

Several different explanations have been proposed for the cold spot. Perhaps the most natural is a large void between us and the last scattering surface [35, 36], which can create the cold spot as a secondary anisotropy via the Rees-Sciamma effect. Such void would have to be 200-300 Mpc/ h in size and have an underdensity of $\delta \sim -0.3$ at redshift of $z \sim 1$. Such large underdensities are extremely unlikely to appear spontaneously in the standard scenario of structure formation.

Alternative proposals include cosmic texture [37, 38], chaotic post-inflationary pre-heating [39], cosmic bubble collisions (e.g., [40]), and nothing less than a gate to extra dimensions [41].

3. Bubble blowing in multi-stream inflation

It is clear that a mechanism that can create nearly circular bubbles or overdensities can provide a plausible explanation of the cold spot. To this end we consider a scenario in which the inflation can experience different number of e-folds at different spatial positions. This can be realized using several different scenarios. Our first example is a two field inflation in which the minimum of the inflaton potential causes spontaneous breaking of the mean-field inflaton path into two distinct paths; an example of such potential is illustrated in Figure

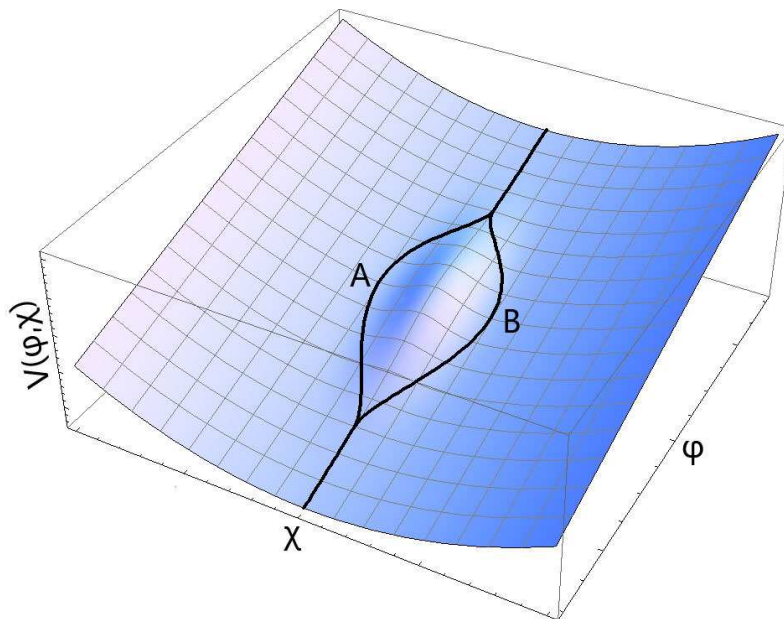


Figure 1: Multi-stream inflation.

1. A similar result can be obtained if inflaton is able to quantum tunnel e.g., from stream A to stream B in the top panel of Figure 1.

We can analyze such scenarios without constructing an explicit inflationary model. The necessary physics is contained in three parameters:

- Probability p that the inflaton will bifurcate (or quantum tunnel) into the path B rather than remaining on the main path A . For perfectly symmetrical bifurcation in the potential $p = 0.5$, but note that this is not necessarily so.
- ΔN_1 is the number of e-foldings at which the bifurcation into paths A and B occurs, after the start of the observable inflation (i.e. ~ 60 e-foldings prior to the end of inflation).
- ΔN_2 is the total difference in the number of e-foldings between the two paths.

These are parameters illustrated in the Figure 2.

In what follows, we will denote the regions that follows path B as bubbles, although the same mechanism can also produce overdense spherical regions. To estimate the number density of such bubbles, we note, that at the time of bifurcation, the number of causally connected regions in the volume corresponding to the present-day observable universe is given by $H_i^{-3} e^{3\Delta N_1} / H_b^{-3}$, where H_i and H_b are the Hubble constants at the beginning of the observable inflation, and the time of bifurcation. Therefore, the total number of bubbles following that path B of the inflation potential is given by

$$N_{\text{observable}} = p (H_b/H_i)^3 e^{3\Delta N_1} = p e^{3(1-\epsilon)\Delta N_1} = p e^{3\Delta N_1^*}, \quad (3.1)$$

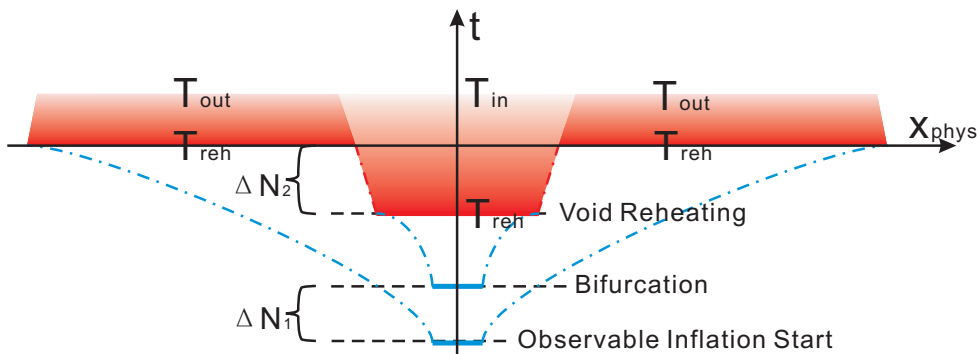


Figure 2: Expansion history for multi-stream inflation.

where we used the definition of the slow-roll parameter ϵ :

$$\epsilon \equiv -\frac{d \ln H}{d \ln a}, \quad \Delta N_1^* \equiv (1 - \epsilon) \Delta N_1 \quad (3.2)$$

assuming that ϵ is roughly constant.

To calculate the physical size of the bubble, we note that the bubble regions reheated ΔN_2 e-foldings earlier and did not exponentially expand while reheating. The comoving radius of individual bubble regions is thus given by

$$R_{\text{bubble}} \sim \left(\frac{1}{H_0} e^{-\Delta N_1^* - \Delta N_2} \right). \quad (3.3)$$

Finally, we want to calculate the density contrast between the bubble and the rest of the universe. In this context, we treat the bubble regions as perturbations in curvature and density. Since the curvature perturbation is conserved outside horizon at all orders, our calculation holds even for significantly underdense bubbles.

We start from the separate universe assumption. When we consider super-Hubble perturbations, the universe within one Hubble volume is locally an FRW universe, with metric

$$ds^2 = \mathcal{N}(\mathbf{x}, t)^2 dt^2 - a^2(t) e^{-2\psi(\mathbf{x}, t)} d\mathbf{x} \cdot d\mathbf{x}, \quad (3.4)$$

where \mathcal{N} and ψ quantify the local physical time/distance with respect to the temporal and spatial coordinates [42, 43]. If perturbations are adiabatic (i.e. pressure is a function of density), energy conservations implies that the curvature perturbation of the uniform density slices :

$$\zeta(\mathbf{x}) = \psi(\mathbf{x}, t) - \frac{1}{3} \int_{\rho_b(t)}^{\rho(\mathbf{x}, t)} \frac{d\rho'}{\rho' + p(\rho')}, \quad (3.5)$$

is conserved and gauge invariant, where $\rho_b(t)$ and $a(t)$ in Eqs. (3.4)-(3.5) are the background (unperturbed) values of density and scale factor. Moreover, $p(\rho) = \rho/3$ after reheating, and $p = 0$ when matter dominates over radiation. One can further show that ζ equals to the e-folding number difference between an uniform density slice and a flat slice. The e-folding number in the flat slice is the same as the background e-folding number. Note that the

reheating surface is a uniform density slice, so on the reheating surface (the surface with temperature T_{reh} in Fig. 2), we have

$$\zeta_* = -(N_{\text{bubble}} - N_0) = \Delta N_2 . \quad (3.6)$$

Note that since ζ_* is a constant, the primordial bubble profile is a top-hat. Moreover, ζ_* is gauge invariant. So in a flat slice, we have

$$\delta\rho = \left(e^{-3(1+w)\Delta N_2} - 1 \right) \rho , \quad (3.7)$$

where $w = 1/3$ when radiation dominates, and $w = 0$ when matter dominates. Also, notice that when the bubble reheats earlier, we have $\Delta N_2 > 0$. In this case, $\delta\rho < 0$. In other words, we are producing underdense regions.

Another important point is that for rare bifurcation events, $p \ll 1$, we expect nearly spherical bubbles. The reason is that the rare peaks of a random gaussian field with a fixed threshold tend to be spherical (e.g., [44]). In our case, the random gaussian field could be the transverse fluctuations about the inflationary trajectory which need to be large to trigger bifurcation.

4. Effects of cosmic bubbles on the CMB

For the calculation of CMB anisotropies, we shall use the linear metric in the Newtonian (or longitudinal) gauge:

$$ds^2 = a^2(\eta) \{ [1 + 2\phi(\mathbf{x}, \eta)] d\eta^2 - [1 - 2\psi(\mathbf{x}, \eta)] d\mathbf{x} \cdot d\mathbf{x} \} , \quad (4.1)$$

where $\phi(\mathbf{x}, \eta)$ and $\psi(\mathbf{x}, \eta)$ are expressed in terms of comoving coordinates \mathbf{x} and conformal time η , which is related to proper time through $dt = a(\eta)d\eta$ (see [45] for comprehensive review of cosmological perturbation theory). Since $\phi = \psi + \mathcal{O}(\psi^2)$ for perfect fluids, for most of what follows (with the notable exception of Rees-Sciama effect), we use $\phi \simeq \psi$.

The gauge-invariant curvature perturbation:

$$\zeta = \psi - \frac{H}{\dot{H}}(H\psi + \dot{\psi}) = \psi + \frac{2(\psi + \dot{\psi}/H)}{3(1+w)} , \quad (4.2)$$

is constant on superhorizon scales during the radiation era, and on all scales in the matter era, and can be derived from Eq. (3.5) (for linear perturbations) using the linearized G_{00} Einstein equation on superhorizon scales:

$$-3H(H\psi + \dot{\psi}) = 4\pi G\delta\rho , \quad (4.3)$$

and Friedmann equation

$$\dot{H} = -4\pi G(\rho + p) . \quad (4.4)$$

Therefore, for the linear Fourier modes $\psi_{\mathbf{k}}$ relevant for the cold spot we can write:

$$\psi_{\mathbf{k}}(t) = g(t)T(|\mathbf{k}|)\zeta_{\mathbf{k}} , \quad (4.5)$$

where $T(k)$ is the transfer function for matter density which goes to 1 on scales bigger than the comoving horizon at matter-radiation transition and $g(t)$ is the homogeneous solution to the equation of ζ conservation (Eq. 4.2), assuming that $\dot{g} = 0$ deep into the radiation era:

$$g + \frac{2(g + \dot{g}/H)}{3(1+w)} = 1. \quad (4.6)$$

During transition between radiation and matter dominated universes, this equation can be solved analytically giving

$$g(a) = \frac{3}{5} + \frac{2}{15}u - \frac{8}{15}u^2 + \frac{16}{15}u^3 \left(\sqrt{1+u^{-1}} - 1 \right), \quad (4.7)$$

where $u = \Omega_{\text{rad}}/\Omega_m a = a_{\text{eq}}/a$. Hence, $g(t)$ goes from $2/3$ in radiation era to $3/5$ in the matter era, and then decays when dark energy starts to dominate. In the transition from matter domination to dark energy domination, the equation must be solved numerically.

4.1 Superhorizon bubbles: Sachs-Wolfe and early ISW effects

To be detectable in the CMB, the bubble should have a superhorizon size if it is close to the last scattering surface. This significantly simplifies the calculations, as the curvature perturbation ζ remains constant. The CMB anisotropies are limited to Sachs-Wolfe and early Integrated Sachs-Wolfe (ISW) effects [46]. The latter is due to the fact that close to the matter-radiation transition the Newtonian potential is varying. The anisotropies are given by:

$$\frac{\delta T(\hat{\mathbf{n}})}{T} = \psi(r_{LSS}\hat{\mathbf{n}}, \eta_{LSS}) + \Theta(r_{LSS}\hat{\mathbf{n}}, \eta_{LSS}) + 2 \int_{\eta_{LSS}}^{\eta_0} d\eta \frac{\partial \psi(\hat{\mathbf{n}}(\eta_0 - \eta), \eta)}{\partial \eta}, \quad (4.8)$$

where $\Theta(\mathbf{x}, \eta)$ is the intrinsic temperature fluctuation in the photon field, while η_0 and η_{LSS} are the conformal times at present and last scattering respectively. Notice that partial derivative in Eq. (4.8) is with respect to conformal time at fixed position, while the integral is over the past light cone, which is why it cannot be taken trivially.

In order to find Θ , we can combine the adiabaticity conditions:

$$\delta \rho_m = 3\rho_m \Theta, \delta \rho_{\text{rad}} = 4\rho_{\text{rad}} \Theta, \quad (4.9)$$

with the superhorizon G_{00} equation (4.3), which yields:

$$\Theta = -\frac{2(\psi + \dot{\psi}/H)}{3(1+w)} = \psi - \zeta, \quad (4.10)$$

using Eq. (4.2). Plugging this in Eq. (4.8), and using:

$$\frac{d}{d\eta} = \frac{\partial}{\partial \eta} + \frac{dr}{d\eta} \hat{\mathbf{n}} \cdot \nabla, \quad (4.11)$$

to replace partial derivative with the total (comoving) derivative, we find:

$$\frac{\delta T(\hat{\mathbf{n}})}{T} = -\zeta(r_{LSS}\hat{\mathbf{n}}) + 2 \int_0^{r_{LSS}} dr \hat{\mathbf{n}} \cdot \nabla \psi(r\hat{\mathbf{n}}, \eta_0 - r). \quad (4.12)$$

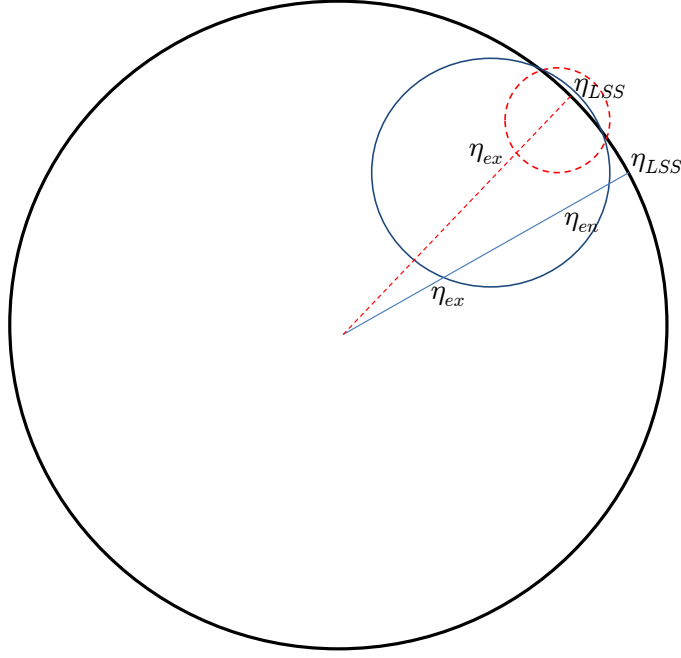


Figure 3: Schematic picture of two bubbles that intersect the last scattering surface. Solid and dashed lines show two typical lines of sight that intersect these bubbles. η_{LSS} , η_{en} , and η_{ex} are conformal times at last scattering, as well as the entry and exit intersections of the line of sight with the bubble.

Given that on superhorizon scales, $\nabla\psi$ is non-vanishing only at the boundaries of the bubble, we can find a closed form for the Sachs-Wolfe + early ISW effects:

$$\left[\frac{\delta T(\hat{\mathbf{n}})}{T} \right]_{SW+e-ISW} = \zeta_* [-\theta(\eta_{LSS} - \eta_{en})\theta(\eta_{ex} - \eta_{LSS}) + 2g(\eta_{ex})\theta(\eta_{ex} - \eta_{LSS}) - 2g(\eta_{en})\theta(\eta_{en} - \eta_{LSS})], \quad (4.13)$$

where η_{en} and η_{ex} are the conformal times at the moments that photon enters and exits the bubble respectively (see Figure 3), while θ is the Heaviside step function. Deep into the matter era, this result reduces to the standard $\zeta_*/5$ for a bubble that intersects the last scattering surface, and vanishes otherwise.

In Figure 4, we plot the profile of such bubble, although note that the edges of this profile will be smoothed on the scale of the sound horizon at last scattering, which is about a degree. In order to find this profile, we find η_{en} and η_{ex} for the line of sight at angle θ from the center of the bubble (Figure 3), use Eq. (4.7) to find $g(\eta_{ex})$ and $g(\eta_{en})$, and plug into Eq. (4.13) to find $\delta T/T$.

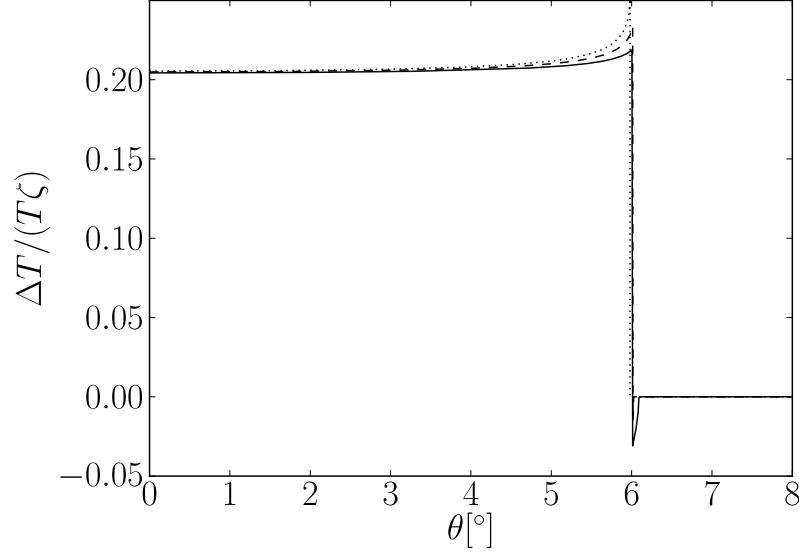


Figure 4: This plot shows the profile of a super-horizon bubble of 1 Gpc/ h radius, centered at $z = 500, 800, 1200$ (solid, dashed, dotted) lines. At small distances from the center of the bubble, the value of g at the photon exit is constant and corresponds to deep matter era. At the lines of sight at the edge of the bubble, g is increasing. At the very edge of the bubble, photons originate outside the bubble for low redshift bubbles and hence the profile reflects the difference in the value of g between bubble entry and exit. The edges of this profile will be smoothed on the scale of the sound horizon at last scattering, which is about a degree.

4.2 Subhorizon bubbles: Late-time ISW and Rees-Sciama effects

For bubbles that had sub-horizon size during the radiation dominated era, the boundaries will not be very sharp as the primordial top-hat profile should be convolved with the transfer function $T(k)$. Assuming linear evolution, and using Eq. (4.5), this implies:

$$\psi(\mathbf{r}, \eta) = g(t)\zeta_* S(|\mathbf{r} - \mathbf{r}_c|), \quad (4.14)$$

$$S(|\mathbf{x}|) = \frac{4\pi R_{\text{bubble}}^3}{3} \int \frac{d^3\mathbf{k}}{(2\pi)^3} \exp(i\mathbf{k} \cdot \mathbf{x}) T(|\mathbf{k}|) W(|\mathbf{k}|R_{\text{bubble}}), \quad (4.15)$$

where

$$W(x) = 3x^{-3}(\sin x - x \cos x), \quad (4.16)$$

is the top-hat filter in the Fourier space. We illustrate this in the Figure 5.

To find the linear late-time ISW effect [46], it is sufficient to assume the bubble profile does not change in a light crossing time. Within this approximation, the impact on the CMB just depends on the projection of the bubble profile $S(r)$:

$$\begin{aligned} \left[\frac{\delta T(b)}{T} \right]_{\text{ISW}} &= 2 \int d\eta \frac{\partial \psi}{\partial \eta} \simeq 2a\dot{g}\zeta_* \int_{-\infty}^{\infty} dy S\left(\sqrt{b^2 + y^2}\right) \\ &= \frac{8\pi a\dot{g}\zeta_* R_{\text{bubble}}^3}{3} \int \frac{d^2\mathbf{k}}{(2\pi)^2} \exp(i\mathbf{k} \cdot \mathbf{b}) T(|\mathbf{k}|) W(|\mathbf{k}|R_{\text{bubble}}), \end{aligned} \quad (4.17)$$

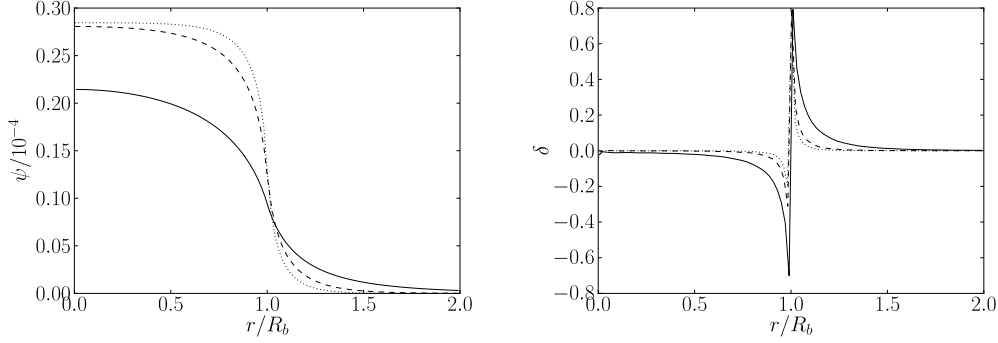


Figure 5: This figure shows the bubble profile in potential (left panel) and overdensity (right panel) for $\zeta_* = 5 \times 10^{-5}$ for bubble size of 100 Mpc/h (solid), 300 Mpc/h (dashed) and 500 Mpc/h (dotted) at redshift $z = 1$. Note that bubbles considered in this paper have the same mean density inside the bubble as the mean cosmic density.

where b is the distance by which the line of sight misses the center of the bubble.

Since the late-time (linear) ISW effect depends on \dot{g} , it only becomes significant when dark energy becomes important. Therefore, since dark energy is sub-dominant at high redshifts, an over/underdensity in the matter era can only contribute to ISW effect at the non-linear level. This is known as the Rees-Sciama effect [47].

In order to find the Rees-Sciama effect, we can use the G_{ij} Einstein equations, deep in the matter era, which take the form:

$$\left[\psi'' + 3aH\psi' + \frac{1}{2}\nabla^2(\phi - \psi) \right] \delta_{ij} - \frac{1}{2}(\phi - \psi)_{,ij} \simeq -4\pi GT_j^i = 4\pi G\rho_m a^2 u^i u^j, \quad (4.18)$$

where $' \equiv \partial_\eta$, while u^i 's are the components of the peculiar velocity, and can be fixed using the matter-era G_{0i} constraint:

$$-H\psi_{,i} = 4\pi G\rho_m a u^i. \quad (4.19)$$

For spherically symmetric scalar fields X ,

$$X_{,ij} = \frac{\partial}{\partial x^j} \left(\frac{\partial X}{\partial r} \frac{\partial r}{\partial x^i} \right) = \frac{x^i x^j}{r} \frac{\partial}{\partial r} \left[r^{-1} \frac{\partial X}{\partial r} \right] \quad (4.20)$$

and hence Eq. (4.19) can be used to write the off-diagonal part of (4.18) as:

$$r \frac{\partial}{\partial r} \left[r^{-1} \frac{\partial(\phi - \psi)}{\partial r} \right] = -\frac{4}{3}(\nabla\psi)^2, \quad (4.21)$$

while its trace takes the form

$$3(\psi'' + 3aH\psi') + r^{-2} \frac{\partial}{\partial r} \left[r^2 \frac{\partial(\phi - \psi)}{\partial r} \right] = \frac{2}{3}(\nabla\psi)^2. \quad (4.22)$$

Equation (4.21) can be integrated using 1st order solution for ψ and inserted into (4.22), yielding an equation for time evolution of ψ' at second order. For fixed $g(t) = 3/5$ in the

matter era, this can be solved to give

$$\psi'^{(2)}(\mathbf{r}, \eta) = \frac{18\zeta_*^2}{175aH} U(|\mathbf{r} - \mathbf{r}_c|), \quad (4.23)$$

where

$$U(r) \equiv \frac{2}{3} \left[\frac{dS(r)}{dr} \right]^2 - \frac{4}{3} \int_r^\infty \frac{dr'}{r'} \left[\frac{dS(r')}{dr'} \right]^2, \quad (4.24)$$

and we have ignored the transient homogeneous solution to Eq. (4.22). Similar to ISW effect, the Rees-Sciama effect is the line of sight integral of ψ' :

$$\left[\frac{\delta T(b)}{T} \right]_{RS} = 2 \int d\eta \psi'^{(2)} = \frac{36\zeta_*^2}{175aH} \int_{-\infty}^\infty dy U(\sqrt{b^2 + y^2}), \quad (4.25)$$

where we have again assumed that the bubble light crossing time is much shorter than the Hubble time. As expected, the total effect is dominated by the ISW contribution at low redshifts and by the Rees-Sciama at higher redshifts.

4.3 Subhorizon bubbles: Ostriker-Vishniac effect

Another secondary anisotropy that could be produced by large bubbles is the Ostriker-Vishniac (or the kinetic Sunyaev-Zel'dovich effect) [48]. This effect is caused by the Doppler shift of the CMB photons, scattered by free electrons in the universe. It is given by:

$$\left[\frac{\delta T(\hat{\mathbf{n}})}{T} \right]_{OV} = - \int_0^{r_{LSS}} dr \frac{d\tau}{dr} [1 + \delta_e(r\hat{\mathbf{n}}, \eta_0 - r)] [\hat{\mathbf{n}} \cdot \mathbf{u}(r\hat{\mathbf{n}}, \eta_0 - r)], \quad (4.26)$$

where δ_e is the overdensity of free electrons, and $d\tau/dr$ is the cosmic mean differential optical depth for Thomson scattering:

$$d\tau = \bar{n}_e a \sigma_T dr. \quad (4.27)$$

Here, \bar{n}_e is the mean physical number density of free electrons in the universe, while σ_T is Thomson cross-section.

On the scales that have not gone through shell-crossing, and assuming a uniform ionization ratio, the electron and total matter overdensities are the same: $\delta_e \simeq \delta_m$. Therefore, G_{0i} Einstein equation:

$$\frac{(ag)'}{g} \psi_{,i} = -4\pi G a^3 \rho_m (1 + \delta_m) u^i, \quad (4.28)$$

can be used to fix the kernel in Eq. (4.26). After integration by part, this yields:

$$\begin{aligned} \left[\frac{\delta T(\hat{\mathbf{n}})}{T} \right]_{OV} &= \frac{f_b(1+X)\sigma_T}{8\pi G m_p} \int_0^{r_{LSS}} dr g^{-1} \psi(r\hat{\mathbf{n}}, \eta) \frac{\partial}{\partial \eta} \left[\frac{x_e}{a^2} \frac{\partial(ag)}{\partial \eta} \right] \\ &\simeq \frac{f_b(1+X)\zeta_*\sigma_T}{8\pi G m_p} \left\{ \frac{\partial}{\partial \eta} \left[\frac{x_e}{a^2} \frac{\partial(ag)}{\partial \eta} \right] \right\} \int_{-\infty}^\infty dy S(\sqrt{b^2 + y^2}) \\ &= \frac{3f_b(1+X)\zeta_*\sigma_T H a^2}{16\pi G m_p} \left\{ \frac{\partial}{\partial a} [x_e H(1-g)(1+w)] \right\} \int_{-\infty}^\infty dy S(\sqrt{b^2 + y^2}), \end{aligned} \quad (4.29)$$

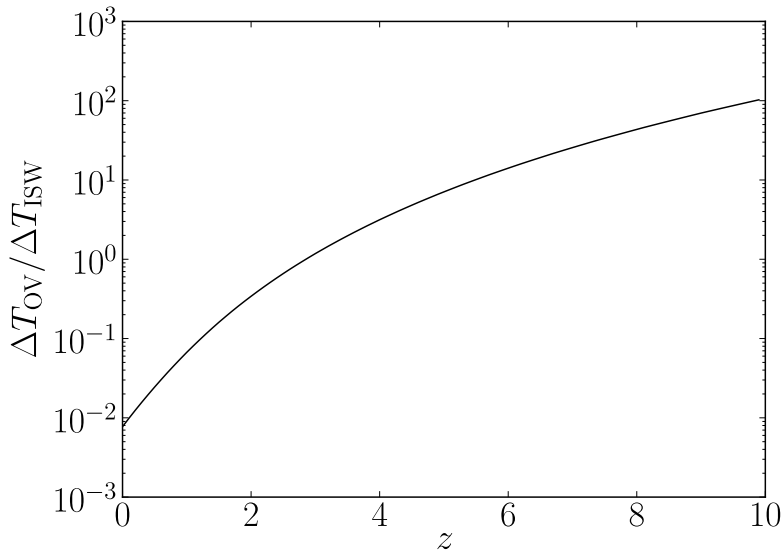


Figure 6: This figure shows the relative amplitudes of Ostriker-Vishniac and ISW effects as a function of redshift. We assume $X = 0.75$ for hydrogen abundance, and fully ionized medium. We ignore the fact that Helium was most likely neutral at redshift bigger than ~ 3 .

where m_p is the proton mass, $X \simeq 0.75$ is the Hydrogen mass fraction in the intragalactic medium, and x_e is the ionized fraction (assuming both hydrogen and helium are ionized equally) and $f_b = \Omega_b/\Omega_m$ is the baryon fraction. H and w are Hubble constant and total equation of state (total pressure divided by total density), respectively.

Since both ISW and OV effects scale as $\zeta_* \int S$, it is easiest to assess the relative strength of the two effects by plotting the ratio of relevant quantities. We do this in the Figure 6. We note that at redshifts of ~ 3 , the two effects become comparable and that for larger redshifts, the OV begins to dominate.

We plot the individual effects discussed here for three representative cases in the Figure 7. The ζ perturbations were chosen to give a perturbation of $\delta T/T \sim 10^{-4}$ which is the same order of magnitude as the cold-spot perturbation. There are several interesting aspects to note regarding these plots. First, the ISW effect dominates at small distances, but never completely overtakes the RS effect for sensible values of ζ that can give the right magnitude. At the same time, the sign of ζ determines whether the two effects are going to interfere constructively or destructively. Second, the ISW and OV effects dominate at small and large redshift respectively and conspire to give similar sized effects. The result is that the total effect has a non-trivial angular structure and redshift dependence and this work provides clear templates that can be tested against real CMB data.

It is interesting to note that a sharp change in the ionization fraction x_e , e.g. at reionization, could also lead to a significant OV effect in Eq. (4.29), as was first pointed out in [49].

Note that, for the purpose of calculation of RS effect in Figure 7, we assumed the

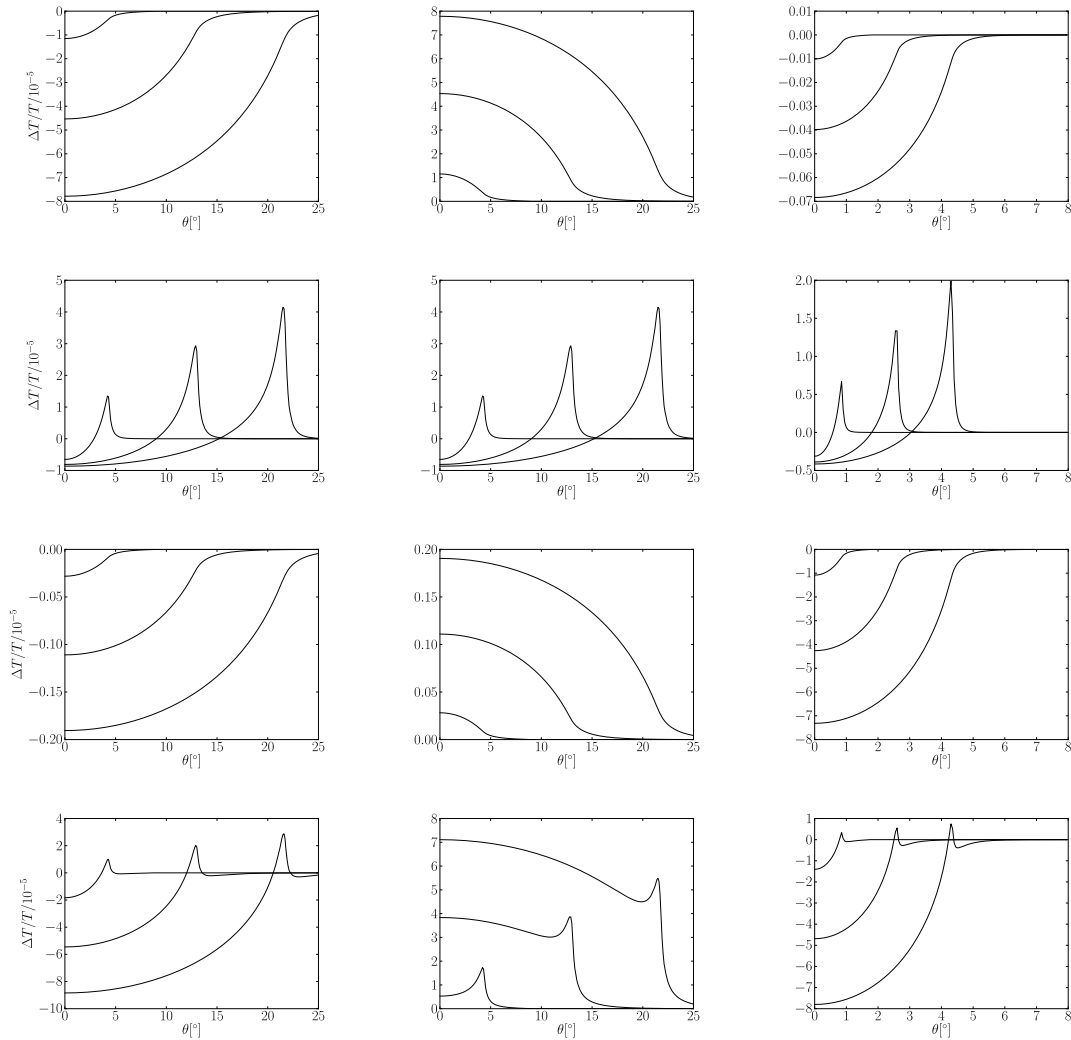


Figure 7: This figure shows the bubble profile associated with ISW (topmost row), Rees-Sciama (second row), Ostriker-Vishniac (third row) and total contribution (bottom row). We show the profile for bubbles size 100, 300 and 500 Mpc/h at redshift $z = 0.5$ with $\zeta_* = 10^{-3}$ (left panels) and $\zeta_* = -10^{-3}$ (middle panels) and at redshift $z = 10$ with $\zeta_* = 10^{-3}$ (right panels).

Universe is still in the matter domination at $z = 0.5$. Given that matter domination ends around $z \sim 0.5$, we expect this assumption to introduce $O(50\%)$ error in RS, and $O(10 - 20\%)$ error in total temperature profile.

5. Comparison with Cold Spot

The mechanism proposed in this section can, in principle, produce bubble regions that can be larger or smaller than the horizon. Therefore, we can explain the bubble using two different scenarios: bubble between us and the surface of the last scattering and a super-horizon overdensity at the actual surface of the last scattering.

If a bubble close to or intersecting the surface of last scattering is responsible for the cold spot, the 4 degree angular radius of the cold spot requires a comoving radius of $R_{\text{bubble}} \sim 1$ Gpc. Figure (4) shows that a temperature decrement of $70 \mu K = 3 \times 10^{-5} T_{\text{CMB}}$ requires $\zeta_* = -1 \times 10^{-4}$. Furthermore, given that there must be one bubble within a Gpc of the last scattering surface (at radius of ~ 10 Gpc), one expect $N_{\text{observable}} \sim 4$ bubbles within our observable horizon. Plugging these into inflationary scenario of Sec. 3 gives:

$$p \sim 0.15, \Delta N_1^* \sim 1, \Delta N_2 \simeq -1 \times 10^{-4}, \text{ for superhorizon bubbles.} \quad (5.1)$$

For bubbles at progressively lower redshifts, the radius of bubble should be smaller to match the observed extent of the cold spot. Given the scarcity of anomalies such as cold spot, we do not expect the bubble to be closer to us than $z \sim 1$, assuming that we sit at a random point in the universe. This gives a minimum radius of ~ 200 Mpc for the bubble, which implies:

$$1 \lesssim \Delta N_1^* \lesssim 4, \quad (5.2)$$

from Eq. (3.3), given that $\Delta N_2 = \zeta_* \ll 1$.

Interestingly, we can also estimate p , simply based on the angular size of the bubble. To do this, we first note that the angular size of the cold spot implies a comoving radius of:

$$R_{\text{bubble}} \sim (1 \text{ Gpc})(r/r_{\text{LSS}}), \quad (5.3)$$

if the bubble sits at the comoving distance r from us. However, if the closest (and thus easiest to see) bubble is at distance r , there should be

$$N_{\text{observable}} \sim (r_{\text{LSS}}/r)^3, \quad (5.4)$$

bubbles within our observable horizon. Now, combining Eqs. (3.1) and (3.3) yields:

$$p \sim N_{\text{observable}} (H_0 R_{\text{bubble}})^3 \sim 0.04, \quad (5.5)$$

given that $H_0^{-1} = 3.0 \text{ Gpc}/h$. In other words, bifurcation into path B is roughly a 2σ event in the inflationary history.

Figures (7) and (6) show that in order to match a temperature decrement of $\sim 10^{-5}$ for bubbles at $0.5 < z < 10$:

$$\zeta_* = \Delta N_2 \sim 10^{-3}, \quad (5.6)$$

i.e. the bifurcated inflationary path (path B) expanded 0.1% more than the regular inflationary trajectory (path A).

Finally, we should note that in what came above we have ignored the impact of regular inflationary gaussian fluctuations on our predictions. The fact is that both Rees-Sciama and Ostriker-Vishniac effects include 2nd order cross-terms with product bubble profile and standard gaussian fluctuations. While these terms have zero mean, they lead to a random component in the bubble profile, which can be potentially seen in higher order statistics of the CMB sky (e.g., see [50, 51]). Such treatment is clearly beyond the scope of the current paper, but will be possible given the formulae provided in Sec. (4).

6. Conclusions and Future Prospects

In this paper we have introduced a novel mechanism that could lead to over/underdense spherical regions/bubbles in the universe, through a probabilistic bifurcation in the inflationary trajectory. We have then worked out predictions for the imprint of such bubbles on the CMB, and estimated approximate values of the parameters of the inflationary scenario that could lead to the observed WMAP cold spot.

If our mechanism is correct and the cold-spot observed in the WMAP data is indeed a massive high redshift bubble, there are several observational probes that can test this assumption:

Of course, the most immediate test will be to investigate how well the CMB profiles of Sec. (4) can fit the WMAP cold spot. Another promising direction is to reconstruct the bubble profile by detecting the lensing of the CMB by the large bubble [52], and compare it to our prediction for density profile (Fig. 5). Such tests are well within realms of experiments such as Atacama Cosmology and South Pole Telescopes [53, 54]. Other tests would include observing changes in the structure formation within such bubble [55]. In fact, using NVSS radio sources, it has been claimed that there is an anomalous underdensity of radio sources coincidental with the position of the cold spot in the CMB [56], but this claim has been discarded upon closer inspection [31]. However, Figure 5 shows that our scenario predicts a compensated bubble wall, rather than a void, which provides a new (and unique) template for comparison with galaxy surveys.

Acknowledgements

We would like to thank Andrei Frolov, Ghazal Geshnizjani, and Tanmay Vachaspati for useful discussions. The authors acknowledge the hospitality of the Kavli Institute for Theoretical Physics in Beijing (KITPC), where this work was originated. The research at KITPC was supported in part by the Project of Knowledge Innovation Program (PKIP) of Chinese Academy of Sciences, Grant No. KJCX2.YW.W10. NA is in part supported by Perimeter Institute (PI) for Theoretical Physics. Research at PI is supported by the Government of Canada through Industry Canada and by the Province of Ontario through the Ministry of Research & Innovation. AS is supported in part by the U.S. Department of Energy under Contract No. DE-AC02-98CH10886. YW is supported in part by Institute of Particle Physics, and by funds from McGill University.

References

- [1] V. F. Mukhanov and G. V. Chibisov, *Quantum fluctuations and a nonsingular universe*, *Journal of Experimental and Theoretical Physics Letters* **33** (May, 1981) 532–535.
- [2] S. W. Hawking, *The development of irregularities in a single bubble inflationary universe*, *Physics Letters B* **115** (Sept., 1982) 295–297.
- [3] A. H. Guth and S.-Y. Pi, *Fluctuations in the new inflationary universe*, *Physical Review Letters* **49** (Oct., 1982) 1110–1113.

- [4] A. A. Starobinsky, *Dynamics of phase transition in the new inflationary universe scenario and generation of perturbations*, *Physics Letters B* **117** (Nov., 1982) 175–178.
- [5] J. M. Bardeen, P. J. Steinhardt, and M. S. Turner, *Spontaneous creation of almost scale-free density perturbations in an inflationary universe*, *Phys. Rev.D* **28** (Aug., 1983) 679–693.
- [6] G. Hinshaw, J. L. Weiland, R. S. Hill, N. Odegard, D. Larson, C. L. Bennett, J. Dunkley, B. Gold, M. R. Greason, N. Jarosik, E. Komatsu, M. R. Nolte, L. Page, D. N. Spergel, E. Wollack, M. Halpern, A. Kogut, M. Limon, S. S. Meyer, G. S. Tucker, and E. L. Wright, *Five-Year Wilkinson Microwave Anisotropy Probe (WMAP) Observations: Data Processing, Sky Maps, and Basic Results*, *ArXiv e-prints* (Mar., 2008) [arXiv:0803.0732].
- [7] E. Komatsu, J. Dunkley, M. R. Nolte, C. L. Bennett, B. Gold, G. Hinshaw, N. Jarosik, D. Larson, M. Limon, L. Page, D. N. Spergel, M. Halpern, R. S. Hill, A. Kogut, S. S. Meyer, G. S. Tucker, J. L. Weiland, E. Wollack, and E. L. Wright, *Five-Year Wilkinson Microwave Anisotropy Probe (WMAP) Observations: Cosmological Interpretation*, *ArXiv e-prints* **803** (Mar., 2008) [arXiv:0803.0547].
- [8] C. L. Bennett, M. Halpern, G. Hinshaw, N. Jarosik, A. Kogut, M. Limon, S. S. Meyer, L. Page, D. N. Spergel, G. S. Tucker, E. Wollack, E. L. Wright, C. Barnes, M. R. Greason, R. S. Hill, E. Komatsu, M. R. Nolte, N. Odegard, H. V. Peiris, L. Verde, and J. L. Weiland, *First-Year Wilkinson Microwave Anisotropy Probe (WMAP) Observations: Preliminary Maps and Basic Results*, *Astrophys. J. Supp.* **148** (Sept., 2003) 1–27.
- [9] M. Cruz, E. Martinez-Gonzalez, P. Vielva, and L. Cayon, *Detection of a non-Gaussian Spot in WMAP*, *Mon. Not. Roy. Astron. Soc.* **356** (2005) 29–40, [astro-ph/0405341].
- [10] A. de Oliveira-Costa and M. Tegmark, *CMB multipole measurements in the presence of foregrounds*, *Phys. Rev.* **D74** (2006) 023005, [astro-ph/0603369].
- [11] C. Copi, D. Huterer, D. Schwarz, and G. Starkman, *The Uncorrelated Universe: Statistical Anisotropy and the Vanishing Angular Correlation Function in WMAP Years 1-3*, *Phys. Rev.* **D75** (2007) 023507, [astro-ph/0605135].
- [12] K. Land and J. Magueijo, *The Axis of Evil revisited*, *Mon. Not. Roy. Astron. Soc.* **378** (2007) 153–158, [astro-ph/0611518].
- [13] D. J. Chung, G. Shiu, and M. Trodden, *Running of the scalar spectral index from inflationary models*, *Phys. Rev.D* **68** (Sept., 2003) 063501–+.
- [14] H. K. Eriksen, F. K. Hansen, A. J. Banday, K. M. Gorski, and P. B. Lilje, “Asymmetries in the CMB anisotropy field.” July, 2003.
- [15] A. Bernui, B. Mota, M. J. Reboucas, and R. Tavakol, *Mapping large-scale anisotropy in the WMAP data*, *Astron. Astrophys.* **464** (2007) 479–485, [astro-ph/0511666].
- [16] J. D. McEwen, M. P. Hobson, A. N. Lasenby, and D. J. Mortlock, *A high-significance detection of non-Gaussianity in the WMAP 5-year data using directional spherical wavelets*, arXiv:0803.2157.
- [17] Y. Wiaux, P. Vielva, R. B. Barreiro, E. Martinez-Gonzalez, and P. Vanderghenst, *Non-Gaussianity analysis on local morphological measures of WMAP data*, arXiv:0706.2346.
- [18] A. Slosar and U. Seljak, *Assessing the effects of foregrounds and sky removal in WMAP*, *ArXiv Astrophysics e-prints* (Apr., 2004) [astro-ph/0404567].

- [19] A. Slosar, U. Seljak, and A. Makarov, *Exact likelihood evaluations and foreground marginalization in low resolution WMAP data*, *ArXiv Astrophysics e-prints* (Mar., 2004) [[astro-ph/0403073](#)].
- [20] M. Li and Y. Wang, *Multi-Stream Inflation*, *JCAP* **0907** (2009) 033, [[arXiv:0903.2123](#)].
- [21] S. Li, Y. Liu, and Y.-S. Piao, *Inflation in Web*, *Phys. Rev.* **D80** (2009) 123535, [[arXiv:0906.3608](#)].
- [22] P. Vielva, E. Martinez-Gonzalez, R. B. Barreiro, J. L. Sanz, and L. Cayon, *Detection of non-Gaussianity in the WMAP 1-year data using spherical wavelets*, *Astrophys. J.* **609** (2004) 22–34, [[astro-ph/0310273](#)].
- [23] **WMAP** Collaboration, C. L. Bennett *et al.*, *First Year Wilkinson Microwave Anisotropy Probe (WMAP) Observations: Preliminary Maps and Basic Results*, *Astrophys. J. Suppl.* **148** (2003) 1, [[astro-ph/0302207](#)].
- [24] E. Martinez-Gonzalez, J. E. Gallegos, F. Argueso, L. Cayon, and J. L. Sanz, *The performance of spherical wavelets to detect non-Gaussianity in the CMB sky*, *Mon. Not. Roy. Astron. Soc.* **336** (2002) 22, [[astro-ph/0111284](#)].
- [25] M. Cruz, L. Cayon, E. Martinez-Gonzalez, P. Vielva, and J. Jin, *The non-Gaussian Cold Spot in the 3-year WMAP data*, *Astrophys. J.* **655** (2007) 11–20, [[astro-ph/0603859](#)].
- [26] L. Cayon, J. Jin, and A. Treaster, *Higher Criticism Statistic: Detecting and Identifying Non-Gaussianity in the WMAP First Year Data*, *Mon. Not. Roy. Astron. Soc.* **362** (2005) 826–832, [[astro-ph/0507246](#)].
- [27] P. Vielva, Y. Wiaux, E. Martinez-Gonzalez, and P. Vanderghelynst, *Alignment and signed-intensity anomalies in WMAP data*, [arXiv:0704.3736](#).
- [28] D. Pietrobon, P. Cabella, A. Balbi, G. de Gasperis, and N. Vittorio, *Constraints on Primordial Non-Gaussianity from a Needlet Analysis of the WMAP-5 Data*, [arXiv:0812.2478](#).
- [29] C. Rath, P. Schuecker, and A. J. Banday, *A Scaling Index Analysis of the WMAP three year data: Signatures of non-Gaussianities and Asymmetries in the CMB*, [astro-ph/0702163](#).
- [30] R. Zhang and D. Huterer, *Disks in the sky: A reassessment of the WMAP 'cold spot'*, *Astropart. Phys.* **33** (2010) 69–74, [[arXiv:0908.3988](#)].
- [31] K. M. Smith and D. Huterer, *No evidence for the cold spot in the NVSS radio survey*, [arXiv:0805.2751](#).
- [32] B. R. Granett, I. Szapudi, and M. C. Neyrinck, *Galaxy Counts on the CMB Cold Spot*, *Astrophys. J.* **714** (2010) 825–833, [[arXiv:0911.2223](#)].
- [33] M. N. Bremer, J. Silk, L. J. M. Davies, and M. D. Lehnert, *A redshift survey towards the CMB Cold Spot*, [arXiv:1004.1178](#).
- [34] M. Cruz, M. Tucci, E. Martinez-Gonzalez, and P. Vielva, *The non-Gaussian Cold Spot in WMAP: significance, morphology and foreground contribution*, *Mon. Not. Roy. Astron. Soc.* **369** (2006) 57–67, [[astro-ph/0601427](#)].
- [35] K. T. Inoue and J. Silk, *Local Voids as the Origin of Large-angle Cosmic Microwave Background Anomalies*, *Astrophys. J.* **648** (2006) 23–30, [[astro-ph/0602478](#)].

- [36] K. T. Inoue and J. Silk, *Local Voids as the Origin of Large-angle Cosmic Microwave Background Anomalies: The Effect of a Cosmological Constant*, *Astrophys. J.* **664** (2007) 650–659, [[astro-ph/0612347](#)].
- [37] M. Cruz, N. Turok, P. Vielva, E. Martinez-Gonzalez, and M. Hobson, *A Cosmic Microwave Background feature consistent with a cosmic texture*, *Science* **318** (2007) 1612–1614, [[arXiv:0710.5737](#)].
- [38] M. Cruz *et al.*, *The CMB cold spot: texture, cluster or void?*, [arXiv:0804.2904](#).
- [39] J. R. Bond, A. V. Frolov, Z. Huang, and L. Kofman, *Non-Gaussian Spikes from Chaotic Billiards in Inflation Preheating*, *Phys. Rev. Lett.* **103** (2009) 071301, [[arXiv:0903.3407](#)].
- [40] B. Czech, M. Kleban, K. Larjo, T. S. Levi, and K. Sigurdson, *Polarizing Bubble Collisions*, [arXiv:1006.0832](#).
- [41] J. A. R. Cembranos, A. de la Cruz-Dombriz, A. Dobado, and A. L. Maroto, *Is the CMB Cold Spot a gate to extra dimensions?*, *JCAP* **0810** (2008) 039, [[arXiv:0803.0694](#)].
- [42] N. Afshordi and R. H. Brandenberger, *Super-Hubble nonlinear perturbations during inflation*, *Phys. Rev.* **D63** (2001) 123505, [[gr-qc/0011075](#)].
- [43] D. H. Lyth, K. A. Malik, and M. Sasaki, *A general proof of the conservation of the curvature perturbation*, *JCAP* **0505** (2005) 004, [[astro-ph/0411220](#)].
- [44] J. M. Bardeen, J. R. Bond, N. Kaiser, and A. S. Szalay, *The Statistics of Peaks of Gaussian Random Fields*, *Astrophys. J.* **304** (1986) 15–61.
- [45] V. F. Mukhanov, H. A. Feldman, and R. H. Brandenberger, *Theory of cosmological perturbations. Part 1. Classical perturbations. Part 2. Quantum theory of perturbations. Part 3. Extensions*, *Phys. Rept.* **215** (1992) 203–333.
- [46] R. K. Sachs and A. M. Wolfe, *Perturbations of a cosmological model and angular variations of the microwave background*, *Astrophys. J.* **147** (1967) 73–90.
- [47] M. J. Rees and D. W. Sciama, *Large-scale Density Inhomogeneities in the Universe*, *Nature* **217** (Feb., 1968) 511–516.
- [48] J. P. Ostriker and E. T. Vishniac, *Generation of microwave background fluctuations from nonlinear perturbations at the era of galaxy formation*, *Astrophys. J. Lett.* **306** (July, 1986) L51–L54.
- [49] M. A. Alvarez, E. Komatsu, O. Dore, and P. R. Shapiro, *The Cosmic Reionization History as Revealed by the CMB Doppler–21-cm Correlation*, *Astrophys. J.* **647** (2006) 840–852, [[astro-ph/0512010](#)].
- [50] I. Masina and A. Notari, *The Cold Spot as a Large Void: Rees-Sciama effect on CMB Power Spectrum and Bispectrum*, *JCAP* **0902** (2009) 019, [[arXiv:0808.1811](#)].
- [51] I. Masina and A. Notari, *The Cold Spot as a Large Void: Lensing Effect on CMB Two and Three Point Correlation Functions*, *JCAP* **0907** (2009) 035, [[arXiv:0905.1073](#)].
- [52] S. Das and D. N. Spergel, *CMB Lensing and the WMAP Cold Spot*, *Phys. Rev.* **D79** (2009) 043007, [[arXiv:0809.4704](#)].
- [53] **The ACT Collaboration**, *et al.*, *The Atacama Cosmology Telescope: A Measurement of the 600j ell j8000 Cosmic Microwave Background Power Spectrum at 148 GHz*, [arXiv:1001.2934](#).

- [54] M. Lueker *et al.*, *Measurements of Secondary Cosmic Microwave Background Anisotropies with the South Pole Telescope*, [arXiv:0912.4317](#).
- [55] A. Cooray and A. Melchiorri, *Small Angular Scale CMB Anisotropies: Early Universe or Local structures ?*, *Phys. Rev.* **D66** (2002) 083001, [[astro-ph/0204250](#)].
- [56] L. Rudnick, S. Brown, and L. R. Williams, *Extragalactic Radio Sources and the WMAP Cold Spot*, *Astrophys. J.* **671** (2007) 40–44, [[arXiv:0704.0908](#)].

